



Article

Efficient Catalytic Degradation of Selected Toxic Dyes by Green Biosynthesized Silver Nanoparticles Using Aqueous Leaf Extract of *Cestrum nocturnum* L.

Pradeep Kumar¹, Jyoti Dixit¹ , Amit Kumar Singh², Vishnu D. Rajput^{3,*} , Pooja Verma¹, Kavindra Nath Tiwari^{1,*} , Sunil Kumar Mishra², Tatiana Minkina³ and Saglara Mandzhieva³

¹ Department of Botany, MMV, Banaras Hindu University, Varanasi 221005, India

² Department of Pharmaceutical Engineering and Technology, Indian Institute of Technology, Banaras Hindu University, Varanasi 221005, India

³ Academy of Biology and Biotechnology, Southern Federal University, 344096 Rostov on Don, Russia

* Correspondence: rvishnu@sfnu.ru (V.D.R.); kntiwaribhu@gmail.com (K.N.T.)

Abstract: In the present study, the catalytic degradation of selected toxic dyes (methylene blue, 4-nitrophenol, 4-nitroaniline, and congo red) using biosynthesized green silver nanoparticles (AgNPs) of *Cestrum nocturnum* L. was successfully performed. These AgNPs are efficiently synthesized when a reaction mixture containing 5 mL of aqueous extract (3%) and 100 mL of silver nitrate (1 mM) is exposed under sunlight for 5 min. The synthesis of AgNPs was confirmed based on the change in the color of the reaction mixture from pale yellow to dark brown, with maximum absorbance at 455 nm. Obtained NPs were characterized by different techniques, i.e., FTIR, XRD, HR-TEM, HR-SEM, SAED, XRD, EDX, AFM, and DLS. Green synthesized AgNPs were nearly mono-dispersed, smooth, spherical, and crystalline in nature. The average size of the maximum number of AgNPs was 77.28 ± 2.801 nm. The reduction of dyes using a good reducing agent (NaBH_4) was tested. A fast catalytic degradation of dyes took place within a short period of time when AgNPs were added in the reaction mixture in the presence of NaBH_4 . As a final recommendation, *Cestrum nocturnum* aqueous leaf extract-mediated AgNPs could be effectively implemented for environmental rehabilitation because of their exceptional performance. This can be utilized in the treatment of industrial wastewater through the breakdown of hazardous dyes.

Keywords: catalytic degradation; dye; DLS; HR-TEM; HR-SEM; AgNPs



Citation: Kumar, P.; Dixit, J.; Singh, A.K.; Rajput, V.D.; Verma, P.; Tiwari, K.N.; Mishra, S.K.; Minkina, T.; Mandzhieva, S. Efficient Catalytic Degradation of Selected Toxic Dyes by Green Biosynthesized Silver Nanoparticles Using Aqueous Leaf Extract of *Cestrum nocturnum* L.. *Nanomaterials* **2022**, *12*, 3851. <https://doi.org/10.3390/nano12213851>

Academic Editor: José Antonio Navío

Received: 28 September 2022

Accepted: 26 October 2022

Published: 31 October 2022

Publisher's Note: MDPI stays neutral with regard to jurisdictional claims in published maps and institutional affiliations.



Copyright: © 2022 by the authors. Licensee MDPI, Basel, Switzerland. This article is an open access article distributed under the terms and conditions of the Creative Commons Attribution (CC BY) license (<https://creativecommons.org/licenses/by/4.0/>).

1. Introduction

Nanotechnology has emerged as an important area of research [1]. The synthesis of nanoparticles (NPs) was motivated by their wide application in fields such as medicine, optics, sensors, and engineering [2]. Physicochemical methods are used in the synthesis of desirable NPs. These methods have limitations in the synthesis of the NPs due to their high cost, the impact of high energy, and the toxicity of the environment. In the present scenario, different metals such as Ag, Au, Pd, Cu, and Zn are used in the synthesis of nanoparticles [3]. Biosynthesized green NPs are preferred due to their low toxicity, biocompatibility, cost-effectiveness, and sustainability for the environment [4–7]. In the biosynthesis of the green NPs, algae [8], fungi [9], bacteria [10], and plant extracts [11] are utilized.

In the green synthesis of AgNPs, plant extracts derived from different natural resources are widely used [12]. These extracts contain various phytochemicals with various functional groups that act as reducing and stabilizing agents [13]. Due to these properties of plant extracts during the green synthesis of AgNPs, no toxic substances are generated, and it can be considered safe to the environment. Water is an important component of life and using in daily life from a variety of sources, including ponds, lakes, rivers, and wells. These aquatic bodies are contaminated with toxic substances such as heavy metals, dyes, pigments,

pesticides, etc., through sewage and industrial effluents. Dyes and pigments are used as coloring agents in the leather, textiles, cosmetics, food, and paper industries [14]. These dyes are exploited on a large scale by the telecommunication industries for fiberoptic technology. It is also used by semiconductor industries for LED and solar cell manufacturing [15].

Dyes are toxic and non-biodegradable, causing mutagenic and carcinogenic effects [16,17]. Due to the high melting point of dyes, their decomposition might be restricted in the soil [18]. As a result of such practices, freshwater tables are contaminated, soil fertility is degraded, and the environment is contaminated. The accumulation of these hazardous compounds in the body causes reproductive toxicity, genotoxicity, mutagenicity, teratogenicity, and neurotoxicity [19]. They also induced changes in genetic material and mitochondrial dysfunction [20].

An appropriate green approach for the environmentally friendly catalytic degradation of dyes is urgently needed to reduce the load of harmful dyes in the ecosystem and to produce less hazardous degradation products of dyes. The present study is focused on the biosynthesis of green AgNPs using the aqueous leaf extract of *Cestrum nocturnum* L. and evaluating its efficacy for the catalytic degradation of synthetic dyes.

2. Materials and Methods

2.1. Chemical Reagents

Silver nitrate (AgNO_3), methylene blue, congo red, 4-nitrophenol and 4-nitroaniline, sodium borohydride (NaBH_4) were purchased from Merck Sigma Aldrich (Burlington, MA, USA).

2.2. Plant Material and Preparation of Extract

Fresh leaves of *Cestrum nocturnum* L. were collected from the campus of Banaras Hindu University, Varanasi, India. The leaves were washed, shade dried at room temperature and grounded to fine powder. The powder was stored in airtight jar at 4 °C. Twenty-five gram of the powdered were added in 100 mL deionized double distilled water and placed on magnetic stirrer at 40 °C for 60 min. The solution was filtered through Whatman filter paper No. 1. Obtained extract was stored as stock solution at 4 °C for further uses.

2.3. Green Synthesis of AgNPs

A reaction mixture was prepared by taking 500 μL of 3% (*v/v*) of *C. nocturnum* aqueous extract (CNAQ) of leaves and mixing it with 5 mL of 1 mM silver nitrate solution. The reaction mixture was exposed to sunlight for a duration of 5 min. The intensity of the incident solar light was 63,000 lx. The color of the reaction mixture changed from pale yellow color to a dark brown color after sunlight exposure. Absorbance of the reaction mixture was measured at different time interval between wavelengths of 250 and 700 nm by the UV-visible spectrophotometer (Shimadzu UV-1800, Tokyo, Japan). After the completion of the reaction, the solution was centrifuged at 12,000 rpm for 10 min. The pellets of the AgNPs were washed with deionized water to remove the impurities associated with AgNPs. It was repeated 2–4 times, and the nanoparticles were dried under vacuum and stored for further use.

2.4. Characterization of Green Synthesized AgNPs

Preliminarily, information regarding the AgNPs biosynthesis emerged from the change in color of the reaction mixture, and further, it was confirmed on the basis of the absorbance of the reaction mixture recorded by UV-Vis spectrophotometer. The particle size and polydispersity index were analyzed by Particulate systems, Nanoplus, Shimadzu. Powder samples of CNAQ and AgNPs were used for FTIR spectroscopy (Bruker, Bremen, Germany) and to investigate the presence of function groups involved in the reduction and encapsulation of Ag^+ ions during the biosynthesis of AgNPs. The XRD pattern of AgNPs was determined by an X-ray diffractometer (Rigaku Miniflex 600), which was equipped with a $\text{Cu K}\alpha$ radiation source and Ni filter in the range of 30–90° at the scanning rate of

2° min^{-1} . High-resolution transmission electron microscopy (HR-TEM) was conducted through Techni G20Twin, FEI at 200 kV. To prepare the sample, a drop of fabricated AgNPs was loaded on a carbon-coated copper grid and dried at $24 \pm 2^\circ \text{ C}$ for 120 min. The sample was mounted onto a specimen holder. The particle size of AgNPs was calculated by Image J software 1.8.0 version. Selected area electron diffraction (SAED) was integrated with HR-TEM to examine the crystalline nature of the NPs. High-resolution scanning electron microscopy (HR-SEM; Nova Nano SEM 450, Moscow, Russia) was used to examine the morphological characteristics of fabricated AgNPs. For imaging, consistently, 1 nA was provided for 7 s at 10 kV. Energy-dispersive X-ray (EDX) was integrated with HR-SEM to examine the elemental make up of AgNPs so that the purity could be predicted. Atomic force microscopy (NT-MDT, Hillsboro Russia) was used to study the topological characteristics of green biosynthesized AgNPs in close proximity. To examine surface properties, a drop of AgNPs solution was mounted over small a glass slide and dried under a table lamp (200 W). AFM images were accessed to calculate the size distribution and roughness profile of AgNPs by Nova software 3.2.5 version.

2.5. Catalytic Reduction in Organic Dyes with Green Synthesized AgNPs

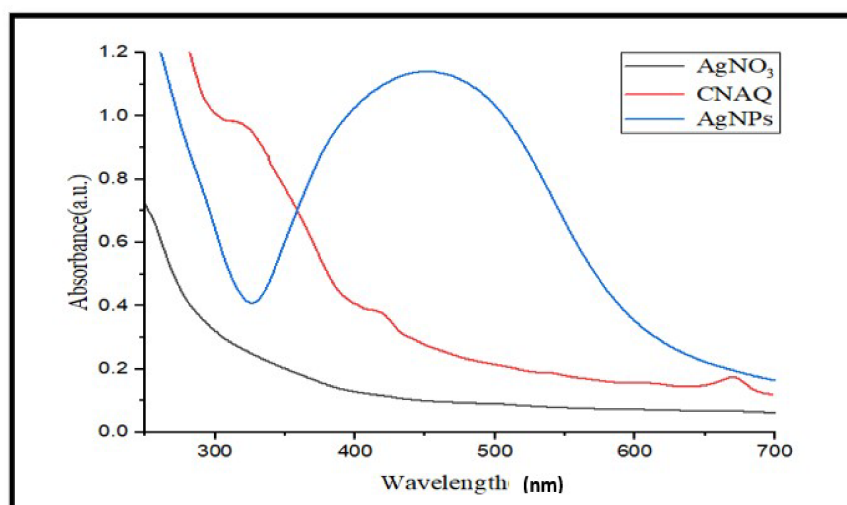
The catalytic activity of green synthesized AgNPs was analyzed for the degradation of organic dyes (methylene blue, congo red, 4-nitrophenol and 4-nitroaniline). To induce the reduction process, NaBH_4 was used as a reducing agent. The reaction mixture was mixed thoroughly, and NaBH_4 was used as a reducing agent. The 4 mL of stock 1 mg/mL of each dye was mixed with 200 μL of 0.5 M NaBH_4 followed by 200 μL of AgNPs. The characteristic spectra of the respective dye were monitored at different time intervals. A control reaction was set up without AgNPs treatment for each dye, and their absorption spectra were recorded with a UV-Vis spectrophotometer (Shimadzu UV 1800, Tokyo, Japan).

3. Results and Discussion

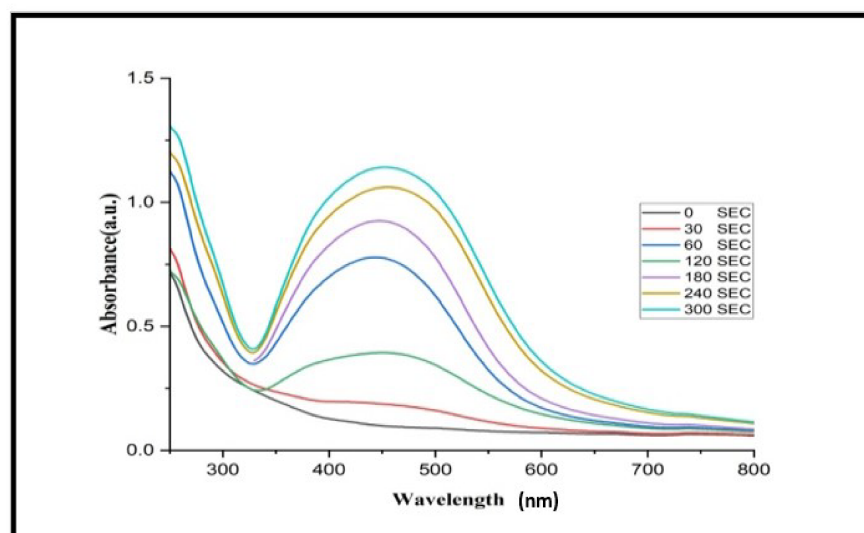
3.1. Biosynthesis of AgNPs and Its Visualization

The absorbance spectra of leaf extract of *C. nocturnum* and green synthesized AgNPs were taken under different wavelengths (Figure 1) [21]. The absorption maxima of leaf extract showed three absorbance peaks at 270, 330, and 423 nm. These peaks might be an indication of polyphenols presence, as they play an important role in the green synthesis of AgNPs [22]. Furthermore, a flask containing the reaction mixture (5 mL of extract (3%) + 100 mL of 1 mM AgNO_3) was kept in sunlight for different time intervals. The change in color of the reaction mixture from pale yellow to brown after sunlight exposure is due to the reduction of Ag^+ ions to metallic Ag. It confirmed the biosynthesis of AgNPs. The maximum absorbance of the reaction mixture was recorded at 250–700 nm. The absorbance between 400–500 nm suggests the biosynthesis of AgNPs.

To optimize the duration of light exposure on the biosynthesis of the AgNPs, the absorbance of the reaction mixture was recorded at 1 min intervals up to 5 min. Results revealed that a strong surface plasmon response (SPR) was recorded at 455 nm (Figure 1A). The excitation of SPR of AgNPs leads to the emergence of brown color and a rise in the intensity of absorption maxima [23]. The height of the absorbance peaks gradually increased with increasing the duration of the light exposure (Figure 1B). It suggests the yield of biosynthesized AgNPs.



A



B

Figure 1. UV-Visible spectra analysis of green synthesized AgNPs. (A) Spectra of aqueous leaf extract of *Cestrum nocturnum* L. (CNAQ), silver nitrate and green synthesized AgNPs, (B) spectra of green synthesized AgNPs at different time intervals (0–300 s), reaction mixture containing 100 mL of silver nitrate (1 mM) and 5 mL inoculum (3% aqueous leaf extract).

3.2. Characterization of AgNPs

3.2.1. Particle Size Distribution

The dynamic light scattering (DLS) method is applied in order to calculate the size distribution as well as the particle diameter profile of microscopic particles that are suspended in a liquid. When a laser beam strikes the circulating NPs, the intensity of the light that is initially entering the system is shifted. This modification was associated with particles. The average particle size was 91.9 nm in diameter, as shown in Figure 2A. The dynamic light scattering (DLS) particle size distribution analysis revealed the polydispersity index (pdi) of green synthesized AgNPs, which was 0.276. It indicates a nearly monodispersed nature of green synthesized AgNPs. The average volume distribution was 56 nm diameter of green synthesized AgNPs (Figure 2B).

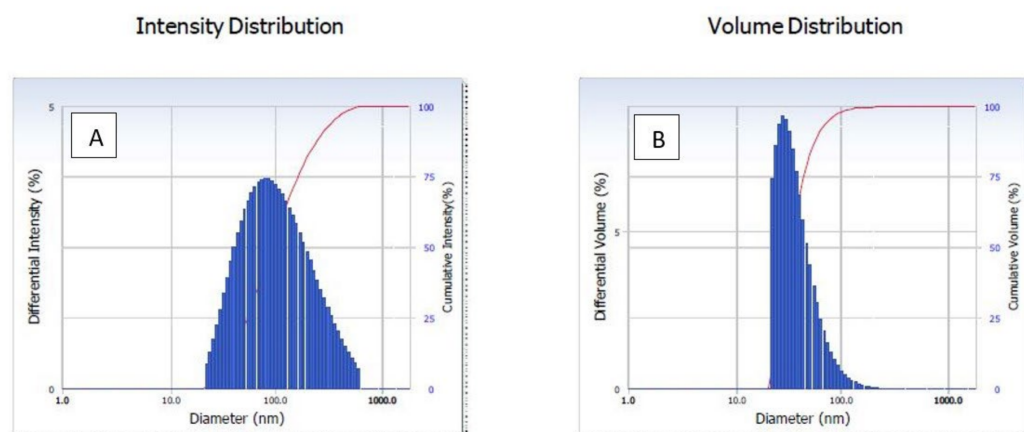


Figure 2. Dynamic light scattering (DLS) of green AgNPs. (A) Intensity, (B) volume distribution of green synthesized AgNPs.

3.2.2. FTIR Spectral Analysis

FTIR analysis of powder of CNAQ revealed the presence of functional groups that participate in the green synthesis of AgNPs. The FTIR spectra of CNAQ and AgNPs were recorded in range $4000\text{--}400\text{ cm}^{-1}$, which is attributed to the signal of stretching vibration of several functional groups (Table 1). FTIR of CNAQ represent peaks at $596, 819.1, 868, 902, 1067, 1230, 1302, 1390, 1486, 1537, 1631, 1761, 2920, 2990,$ and 3416 cm^{-1} . In the AgNPs FTIR spectra, these peaks were shifted to $589.6, 794.5, 846.2, 889.5, 1053, 1197, 1287, 1385, 1494, 1545, 1619, 1777, 2920, 2984$ and 3410 cm^{-1} (Figure 3). The broad peak at 1385 cm^{-1} detected in AgNPs corresponds to the intense vibration of NO in the NO_3^- . The intensity of these peaks was decreased and shifted in the spectra of the AgNPs. Similar results were reported in *Premna integrifolia* mediated AgNPs [24]. The above finding reveals that most of the peaks such as $868, 1067, 1486, 1631,$ and 3416 cm^{-1} represent the flavonoid group of compounds [25,26]. The reduction and shifting of these peaks suggests the involvement of these groups in the biosynthesis of the AgNPs (Table 1). It means flavonoid-rich extract of leaves participated in the biosynthesis and stabilization of the green AgNPs.

Table 1. FTIR profiling of CNAQ and AgNPs.

| Frequency (cm^{-1}) | Peak Wavenumber | | Functional Group/Type of Bond | Compounds |
|-----------------------------------|-----------------|-------|----------------------------------|---|
| | CNAQ | AgNPs | | |
| 3550–3200 | 3416 | 3410 | O-H stretching | Phenol, hydroxy compound |
| 3200–2500 | 2990 | 2984 | O-H stretching | Carboxylic acid |
| | 2920 | 2920 | O-H stretching | Carboxylic acid |
| 2000–1650 | 1761 | 1777 | C-H bending | Aromatic compounds |
| 1680–1600 | 1631 | 1619 | C=C stretching | Alkenes |
| 1625–1440 | 1537 | 1545 | C=C stretching | Aromatic compounds |
| 1490–1410 | 1486 | 1494 | Carbonate ion | Inorganic compounds |
| 1420–1300 | 1302 | 1287 | Carboxylate | Carbonyl compounds |
| 1250–1020 | 1230 | 1197 | -C-N- stretching | Aliphatic amines |
| 1140–1070 | 1068 | 1053 | C-O stretching | Cyclic ether and oxy group of compounds |
| 1000–600 | 902 | 889.5 | C-H stretching | Alkenes |
| | 868 | 846.2 | C-H stretching | Alkenes |
| | 819.1 | 794.5 | C-H stretching | Alkenes |
| 720–590 | 596.4 | 589.5 | O-H out of plane bend | Hydroxy compounds |

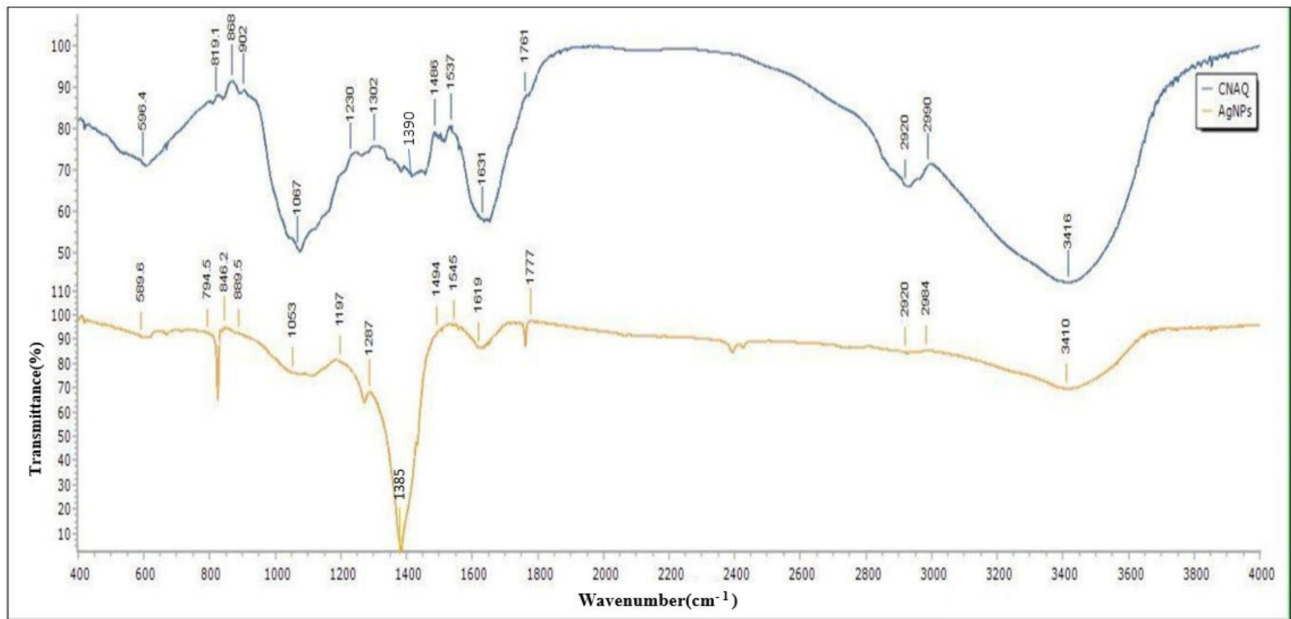


Figure 3. FTIR spectra of the CNAQ and AgNPs.

3.2.3. XRD

The XRD pattern of green synthesized AgNPs showed the diffraction peaks at 38.19° , 44.38° , 64.47° , 77.41° , and 81.55° , which are attributed to (111), (200), (220), (311), and (222) Bragg reflections, respectively (JCPDS file no. 00-004-0783). These Bragg reflections are corresponded to the crystalline planes of the face-centered cubic (fcc) crystal lattice of metallic silver (Figure 4). Similar crystalline peaks at 32.28° , 46.28° , 54.83° , 67.47° were observed by other workers [27,28]. The stronger planes indicate silver as a major constituent in biosynthesized green AgNPs. In the XRD spectra of AgNPs, several small not indexed peaks such as 32.31° , 32.80° and 54.97° are denoted by an (*) symbol. Peaks 32.31° and 32.80° represented organic compounds of CNAQ, while 54.97° denoted silver oxide. Similar results were reported in *Clinacanthus nutans* [29], *Ananas comosus* [30] and *Carob* mediated AgNPs [31].

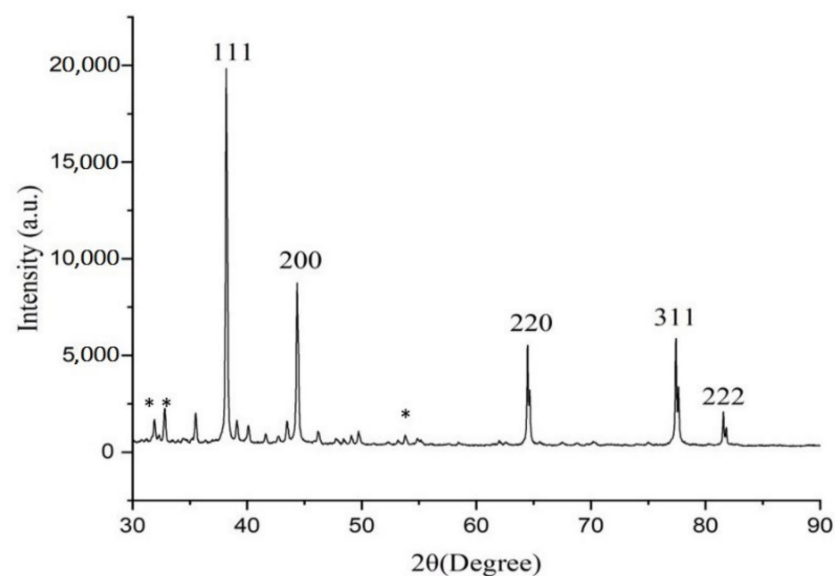


Figure 4. XRD pattern of AgNPs. Star (*) symbol represents small not indexed peaks such as 32.31° , 32.80° and 54.97° .

3.2.4. HR-TEM and SAED

High-resolution transmission electron microscopy is widely used to study the size, shape and morphology of green synthesized AgNPs [15]. HR-TEM images revealed that green synthesized AgNPs were uniformly dispersed and spherical in shape (Figure 5A). Selected area electron diffraction analysis (SAED) of AgNPs depicted a bright circular ring, which revealed its highly crystalline nature (Figure 5B). SAED is commonly used to confirm the crystallinity of the AgNPs [32]. The size of synthesized AgNPs was distributed in the range of 50–95 nm (Figure 5C). The size distribution histogram (Figure 5C) confirmed the average size of the maximum number of green synthesized AgNPs was 77.28 ± 2.801 nm.

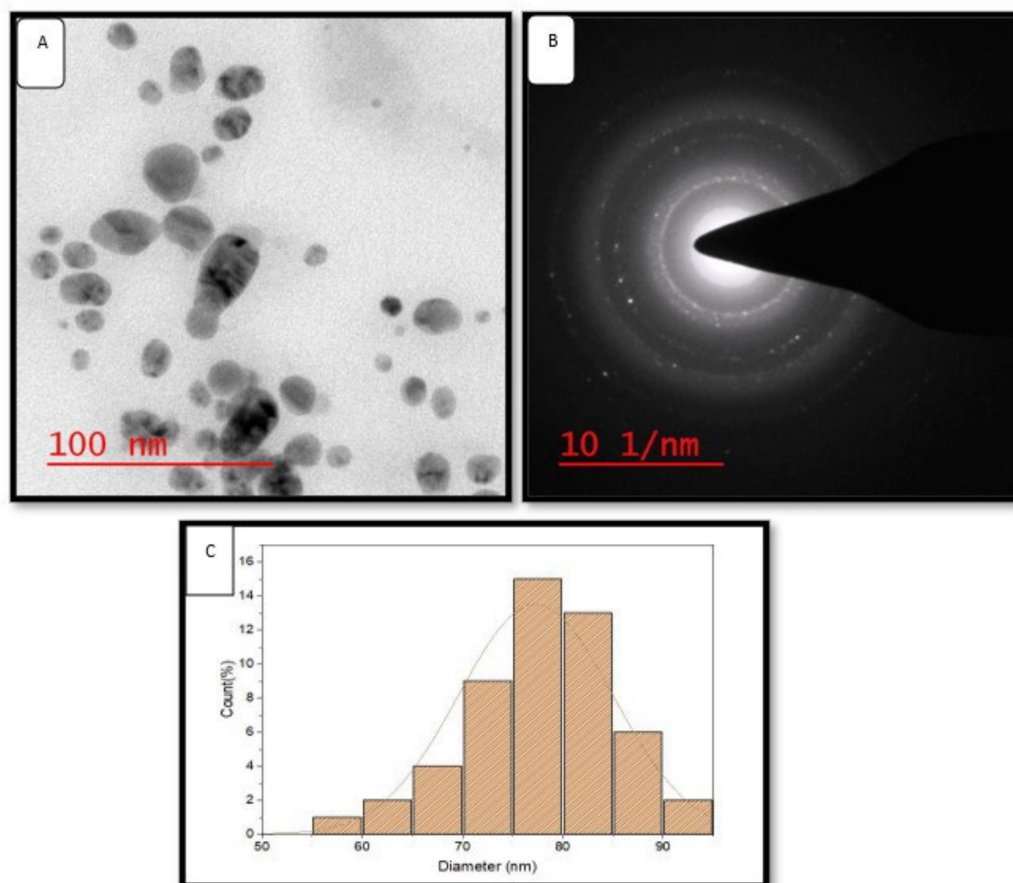


Figure 5. HR-TEM images of green AgNPs. (A) HR-TEM images of green AgNPs at 200 nm, (B) SAED patterns of green AgNPs, (C) size distribution histogram of green AgNPs.

3.2.5. HR-SEM and EDX

A high-resolution scanning electron micrograph depicted the surface morphology of green synthesized AgNPs [33]. HR-SEM data analysis revealed that green synthesized AgNPs varied in size. Biosynthesized AgNPs were smooth and spherical in shape (Figure 6A). Images showed that green synthesized AgNPs formed aggregates (Figure 6B). The aggregation of nanoparticles might be due to protein, carbohydrates, and glycoprotein present in the plant constituents. EDX of green synthesized AgNPs showed the presence of silver (Ag). The sharp peak at 3 keV indicated the presence of metallic Ag (Figure 6C). Additional peaks (C, O, Na, and Si) might be because of glass, as the sample was coated on it.

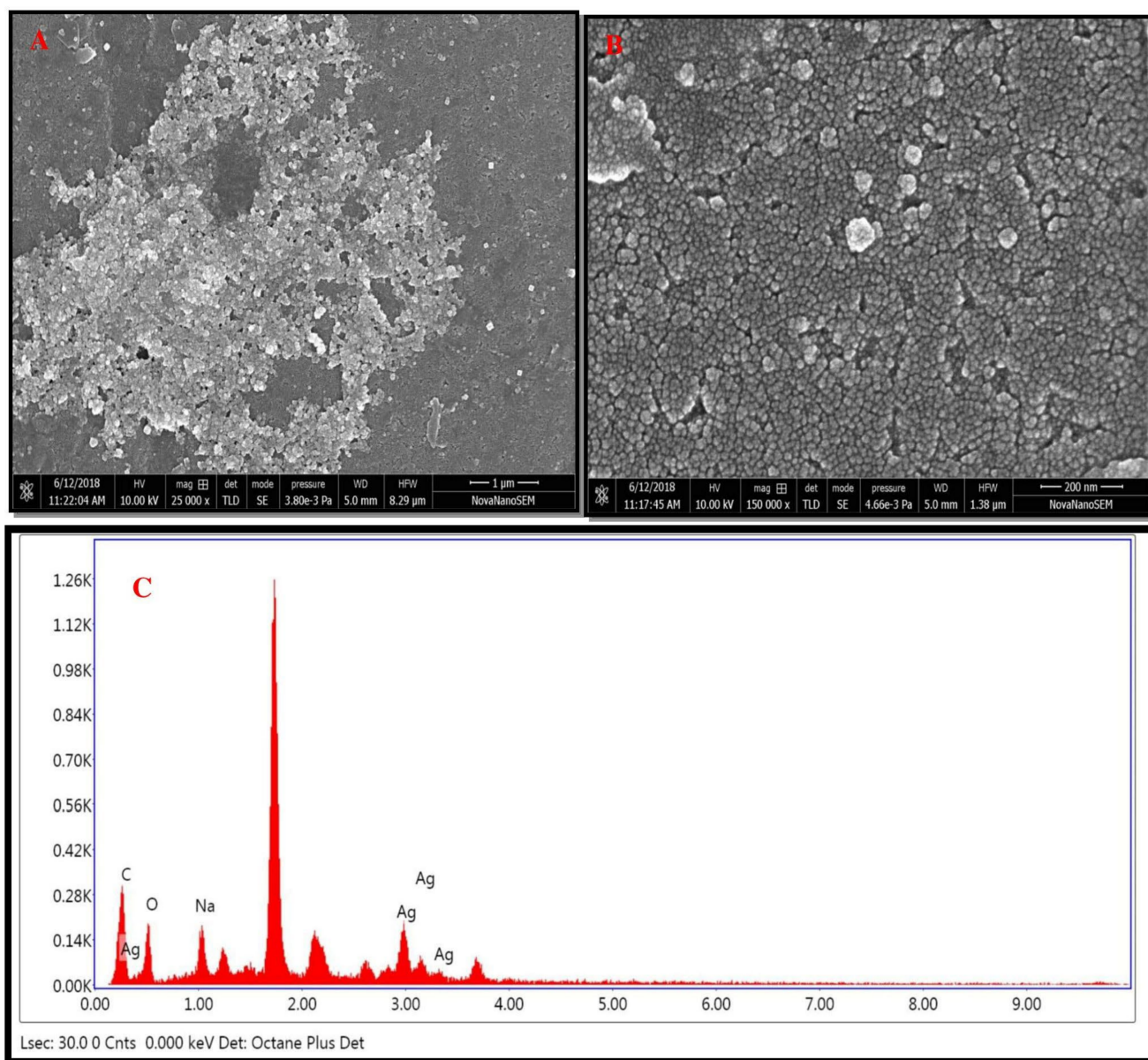


Figure 6. HR-SEM images of green AgNPs. (A) HR-SEM images of green AgNPs at 1 μm , (B) HR-SEM images of green AgNPs at 200 nm, (C) and EDX spectrum of green synthesized AgNPs.

3.2.6. AFM

Topographical features of green synthesized AgNPs were examined by atomic force microscopy [34]. The 2D (Figure 7A) and 3D (Figure 7C) images revealed the spherical nature of green synthesized AgNPs, which is correlated with HR-TEM and HR-SEM outcomes. The roughness of biosynthesized AgNPs was very clear, as given in Figure 7B,C. Image analysis using Nova software, including the average roughness, maximum profile peak height, and valley depth of AgNPs, was calculated. The average roughness of green synthesized AgNPs was 10.12 nm (Figure 7B). The maximum profile peak height and valley depths were 18.327 nm and 23.405 nm, respectively, in the 2D image. In the 3D image, the average roughness of green synthesized AgNPs was 14.41 nm, while the maximum profile peak height and valley depth was reported 47.73 nm and 55.07 nm, respectively (Figure 7D).

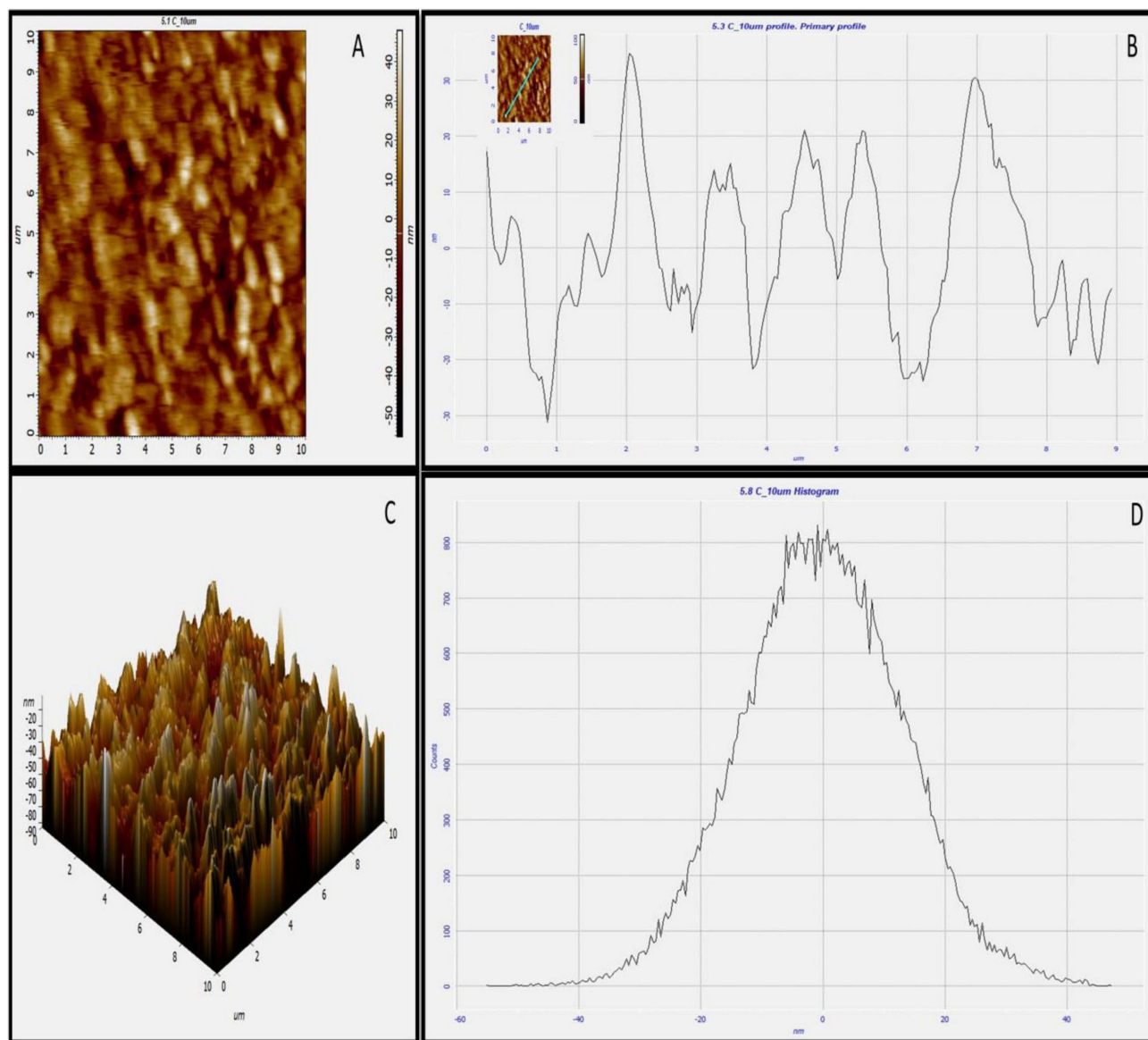


Figure 7. AFM images of green synthesized AgNPs. (A) Two-dimensional (2D) image of green AgNPs, (B) 2D roughness profile of green AgNPs, (C) 3D image of green AgNPs, (D) 3D roughness profile of green AgNPs.

3.3. Mechanism of Biosynthesis of the AgNPs

CNAQ is rich in many bioactive compounds such as flavonoids, steroids, glycosides, triterpenes, caffeoyl derivatives, and other aromatic compounds [35,36]. Proteins, glucose, and other bioactive components found in the leaf extract serve as strong capping agents for AgNPs formation, while flavonoids act as effective reducing agents [37,38]. A possible mechanism of the biosynthesis of AgNPs by using bioactive compounds of the CNAQ is given in Figure 8. During AgNPs biosynthesis, a reduction of Ag^+ to Ag^0 took place by several phytochemicals present in CNAQ, particularly flavonoids present in the extract acting as a strong reducing agent [29]. Quercetrin is an important photoactive flavonoid with a huge number of -OH groups present in the extract. The phenylpropanoid pathway produces quercetrin, which is finally formed from phenylalanine. When kept under solar radiation, during the reaction mixture, the release of two electrons from -OH groups of quercetrin takes place, which are used in the reduction process of Ag^+ to Ag^0 . Furthermore, it catalyzes the biosynthesis of AgNPs. This assumption was supported by the IR examina-

tion, which revealed that the -OH groups are involved in the synthesis and stabilization of AgNPs.

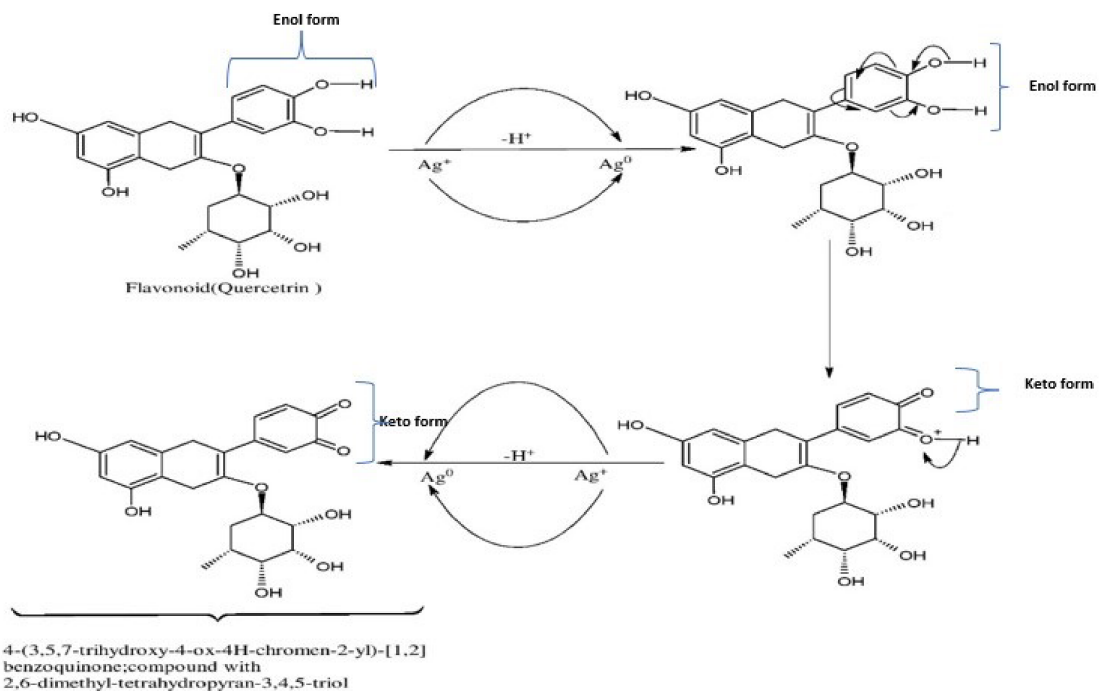


Figure 8. Biosynthesis mechanism of the AgNPs through involvement of the flavonoid (Quercitrin) present in CNAQ.

The charge-transfer-induced conformational modifications in the flavonoids (quercitrin) during the reduction of Ag^+ to Ag^0 . The elimination of two hydrogen atoms of the enol form and the deduction of two electrons are capable of reducing 2Ag^+ to 2Ag^0 , accelerating the synthesis of AgNPs [33].

3.4. Catalytic Degradation of Dyes by Green AgNPs

Dyes are colored compounds extensively used to color the products of a wide range of industries. Industrial effluents contain these dyes. Every year, approximately 7×10^5 tonnes of synthetic dyes are used worldwide [39]. Dyes-based effluents cause a serious hazard to the water stream and environment due to their synthetic origin and complex molecular structure, which decreases their ability to biodegrade. The release of the effluents into the aquatic environment without sufficient treatment generates detrimental effects on the qualities of the aquatic bodies such as biological oxygen demand (BOD), chemical oxygen demand (COD), color, heavy metal content, penetration of light and other properties. Several traditional treatment techniques, such as UV-light degradation, flocculation, activated carbon sorption, redox treatment, and electrocoagulation, have been used for degradation of the effluent [40]. These techniques are costly, time consuming, and produce by-products. In order to reduce these challenges, researchers are focusing on natural substitutes for the degradation of synthetic dyes [41]. Biological treatments are the ideal techniques for improving the quality of the effluents because they are cost-effective and efficient. Using green nanoparticles might be a good way to get rid of hazardous dyes for environmental remediation.

Methylene blue belongs to the phenothiazine dye class. It decomposes at 100–110 °C [20]. It showed a maximum absorption peak at 664 nm. The control experiment containing NaBH_4 and methylene blue solution did not show a significant change in the blue color of the solution as well as a decrease in absorption spectra with respect to time (Figure 9(iA)). The addition of AgNPs to the reaction mixture (methylene blue and NaBH_4) completely decolorized the dye from blue color to colorless. The absorption spectra of methylene blue

(664 nm) also disappeared within 8 min (Figure 9(iB)). The catalytic degradation percentage of methylene blue was 15% in the presence of NaBH_4 (Figure 9(iC)), while the catalytic degradation percentage, was 79% within 8 min, when AgNPs was added to methylene blue and NaBH_4 solution (Figure 9(iD)). The results showed that AgNPs in the presence of NaBH_4 catalyzed the complete reduction of methylene blue into leuco methylene blue in the presence of NaBH_4 [42]. Similar results were reported in AgNPs of *Thymbra* [22], *Trigonella foenum-graecum* [43], and the fruits of *Terminalia chebula* [44], indicating their nanocatalyst potential for the reduction of methylene blue.

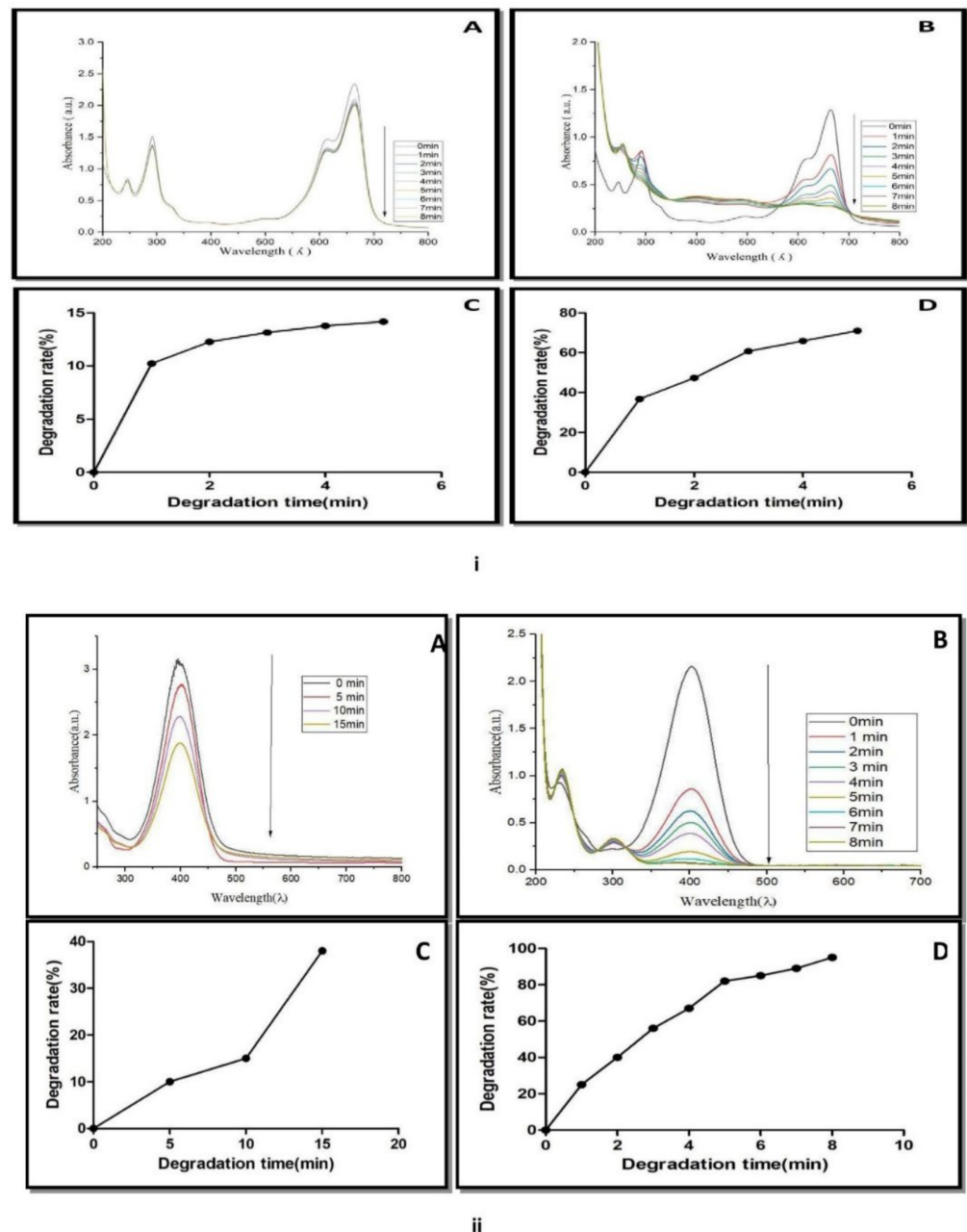


Figure 9. (i) UV-Vis spectra of methylene blue reduction in presence of (A) NaBH_4 , (B) NaBH_4 + green biosynthesized AgNPs. (C) Catalytic degradation (%) of methylene blue in the presence of NaBH_4 . (D) Catalytic degradation (%) with NaBH_4 + AgNPs. (ii) UV-Vis spectra of 4-nitro phenol reduction in the presence of (A) NaBH_4 , (B) NaBH_4 + green biosynthesized AgNPs, (C) catalytic degradation (%) with NaBH_4 . (D) Catalytic degradation (%) with NaBH_4 + AgNPs.

The nanocatalytic reduction of dye at 1 mg mL^{-1} concentration was studied by observing the change in the characteristic absorption spectra of 4-nitrophenol dye. 4-Nitrophenol ($\text{C}_6\text{H}_5\text{NO}_3$) is also known as p-nitrophenol or 4-hydroxy nitro-benzene. It is a phenolic molecule with a nitro group and a hydroxyl group at the benzene ring. 4-Nitrophenol is widely used for the production of several drugs, including acetaminophen, fungicides, and insecticides (methyl and ethyl parathion). It is also used for leather darkening and as a coloring agent [45]. When 4-nitrophenol is mixed with sodium borohydride (NaBH_4), the absorption spectra slowly decreased within 0–15 min (Figure 9(iiA)). NaBH_4 did not show a significant change in yellow color of 4-nitrophenol. The reduction of 4-nitrophenol by NaBH_4 was approximately 39% (Figure 9(iiC)).

It means that 4-nitrophenol is not completely converted into 4-aminophenol. AgNPs catalyzed the fast reduction of 4-nitrophenol into 4-aminophenol when it was added to a reaction mixture containing 4-nitrophenol and NaBH_4 . After the addition of AgNPs to the reaction mixture, a rapid decline in absorption spectra was recorded (Figure 9(iiB)). A new spectrum appeared at 300 nm during the conversion. The decline of the absorption spectrum at 400 nm and the appearance of new spectra at 300 nm revealed the complete reduction of the 4-nitrophenol into 4-aminophenol within 8 min. Approximately 92% of the 4-nitrophenol is transformed into 4-aminophenol within 8 min (Figure 9(iiD)). A similar result was reported by several plant such as *Dillenia indica* bark extract [46], leaf extract of *Euphorbia heterophylla* [47] and other plant-mediated AgNPs in the degradation of 4-nitrophenol [48]. These reports concluded that the appearance of the new peak at 300 nm was due to the conversion of the $-\text{NO}_2$ to $-\text{NH}_2$. 4-Nitroaniline ($\text{C}_6\text{H}_6\text{N}_2\text{O}_2$) is another important dye known as p-nitroaniline or 1-amino-4-nitrobenzene. It is a yellow and amorphous organic dye.

It is used as a corrosion inhibitor and an intermediary in the manufacturing of colors, medicines, fuels, and poultry pharmaceuticals [49]. The catalytic reduction of 4-nitroaniline was analyzed with or without AgNPs in the presence of NaBH_4 . The maximum absorption spectrum of dye was 382 nm. NaBH_4 was added to the dye solution, and there was also a reduction in the absorption spectrum and a slight change in the yellow color of the dye solution occurred.

This suggests the slow catalytic degradation of the 4-nitroaniline in the presence of NaBH_4 (Figure 10(iA)). It was also noted that there was no significant change in the absorption spectrum of 4-nitroaniline within 30 min. The addition of AgNPs in the mixture of dye and NaBH_4 solution resulted in the disappearance of the absorption spectra at 382 nm and the decolorization of 4-nitroaniline (Figure 10(iB)). The percentage of 4-nitroaniline degradation was 18% by NaBH_4 (Figure 10(iC)), while its degradation was increased to 78% by NaBH_4 and AgNPs (Figure 10(iD)). Similar results were reported in Citrus aurantifolia peel extract derived silver nanoparticles.

The change in the color of the dye from yellow to colorless was observed after the addition of green biosynthesized nanoparticles. It means that the conversion of 4-nitroaniline took place into 4-aminoaniline. A similar result regarding the degradation of 4-nitroaniline by biosynthesizing green nanoparticles was reported by Sarvalkar et al. (2021) [50]. Congo red ($\text{C}_{32}\text{H}_{22}\text{N}_6\text{Na}_2\text{O}_6\text{S}_2$) belongs to the azo dye class. It showed two characteristic absorption peaks at 490 nm and 330 nm (Figure 10(iiA,B)). The formation of two different absorption peaks at 490 nm and 330 nm is due to electron transitions from $\pi \rightarrow \pi^*$ and $n \rightarrow \pi^*$ respectively. The catalytic degradation of congo red was observed for up to 30 min in the presence of NaBH_4 (Figure 10(iiA)). Results revealed that the change in absorption spectrum was very slow. It suggests a very slow catalytic degradation of congo red by NaBH_4 (Figure 10(iiC)). The degradation of dye in the presence of AgNPs was monitored, and a change in absorption spectrum was noted between 0 and 15 min (Figure 10(iiB)). The addition of AgNPs to the reaction mixture of congo red and NaBH_4 synergistically enhanced the reduction of dye, leading to a change in the color of the reaction mixture from red to colorless within 15 min. It also demonstrated the disappearance of both absorption peaks (490 nm and 330 nm) and dye degradation up to 80% within 15 min (Figure 10(iiD)).

Similar results were reported in *Amaranthus gangeticus* [51] and *Anacardium occidentale* [52] extract-mediated AgNPs. The degradation mechanism of methylene blue, 4-nitrophenol, 4-nitroaniline and congo red are shown in Figure 11A–D.

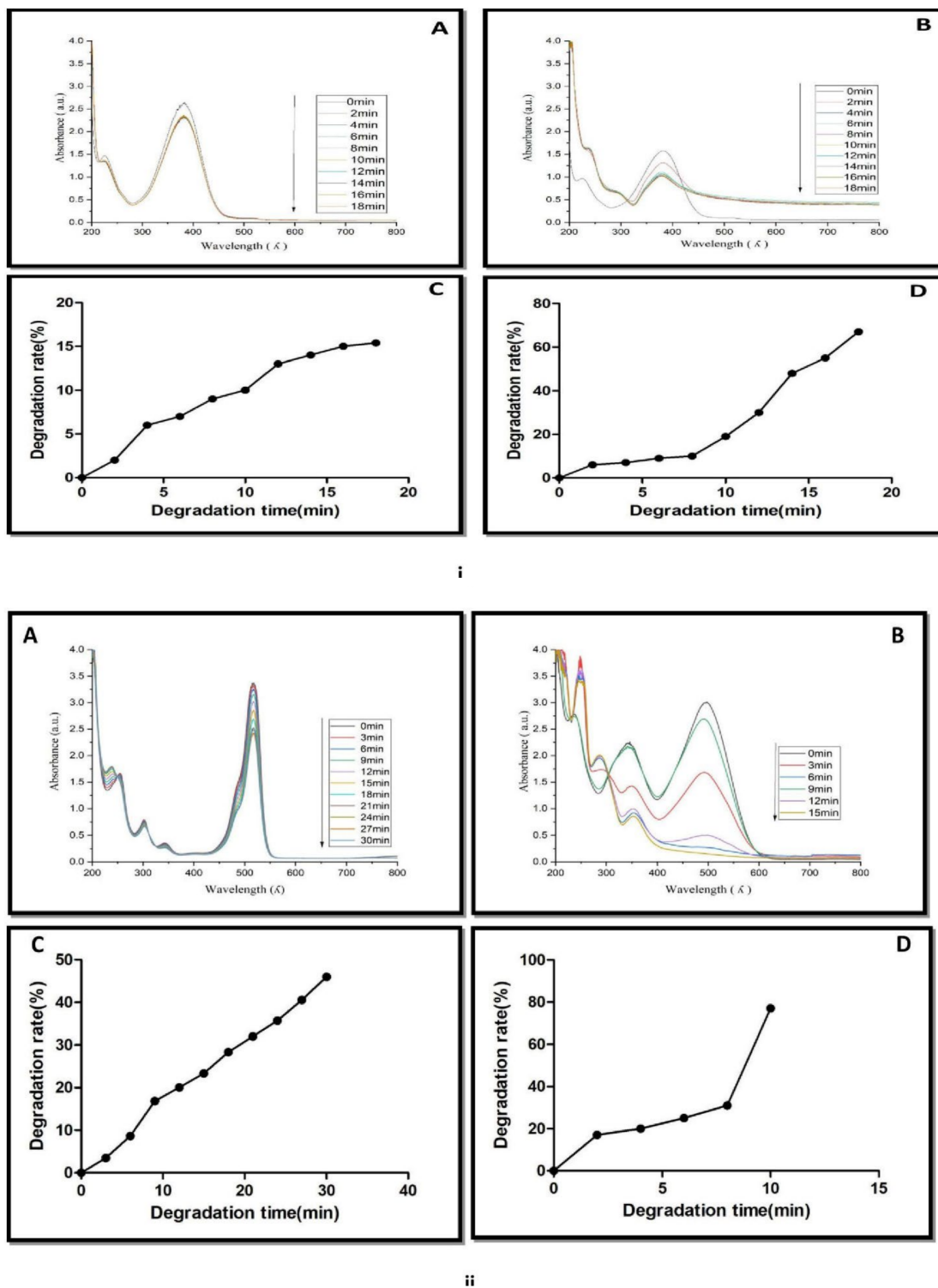


Figure 10. (i) UV-Vis spectra of 4-nitroaniline reduction in presence of (A) NaBH₄, (B) NaBH₄ + green biosynthesized AgNPs, (C) Catalytic degradation (%) with NaBH₄. (D) Catalytic degradation (%) with NaBH₄ + AgNPs. (ii) UV-Vis spectra of congo red reduction in presence of (A) NaBH₄ and (B) NaBH₄ + green biosynthesized AgNPs. (C) Catalytic degradation (%) with NaBH₄. (D) Catalytic degradation (%) with NaBH₄ + AgNPs.

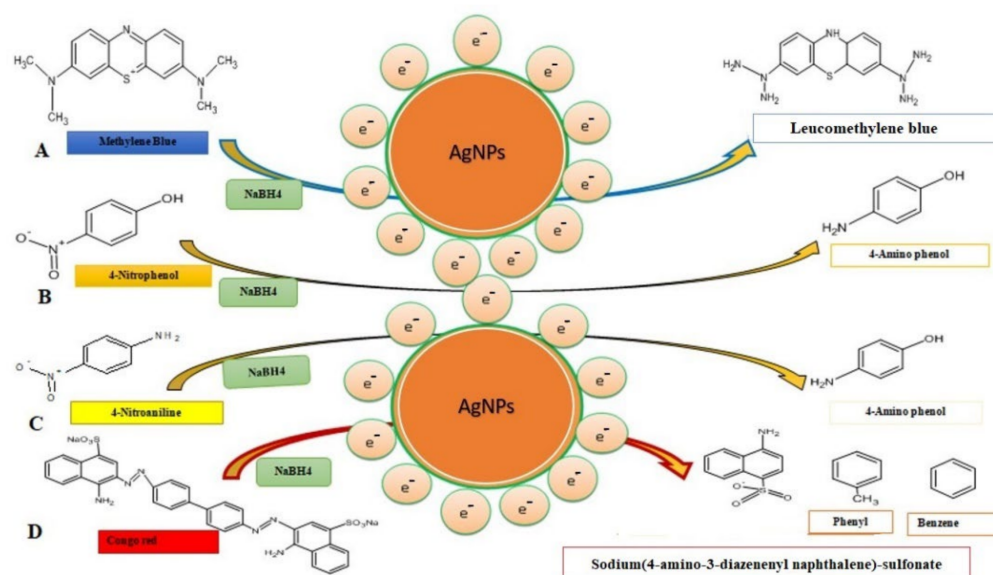


Figure 11. Degradation mechanism of toxic dyes and their catalytic degradation products through the involvement of the AgNPs. (A) Methylene blue, (B) 4-nitrophenol, (C) 4-nitroaniline, and (D) congo red.

It might be possible that AgNPs mediated the breakage of the $-N=N-$ double bond of the chromophore group of azo dye into sodium (4 amino-3-diazenylnaphthalene) sulfonate, phenyl, and benzene due to which the reaction mixture turned colorless. The result obtained was in accordance with the catalytic degradation of a variety of dyes in water by recyclable nano catalysts [22]. The degradation of dye was a thermodynamically spontaneous reaction that required large free energy. Due to the large transition energy gap between an electron donor (NaBH_4) and an electron acceptor (dye), no electron transfer was facilitated [53]. Silver nanoparticles catalyzed heterogeneous catalysis reactions. As a result, green synthesized silver nanoparticles have a high surface to volume ratio. Thus, these nanoparticles have been used for a variety of uses [54]. The mechanism of catalytic degradation of dye through silver nanoparticles involves electron transfer and the least activation energy [55].

For the purpose of reducing the dyes, AgNPs serve as electron relays, allowing for the transfer of electrons from the BH_4^- -ion toward the dye. At the same time that the NPs' surfaces were becoming saturated with BH_4^- -ions, electron transfer from the ion to the dye was taking place [56]. Silver nanoparticles assisted the transfer of electrons from reducing agent BH_4^- to dye and lead to the disintegration of the chromophore structure of dye into small molecules [57]. They reduce the kinetic barrier between the nucleophilic NaBH_4 and electrophilic dye as a redox catalyst.

It has been observed that certain additional nanomaterials, such as $\text{Au/g-C}_3\text{N}_4/\text{Co}_3\text{O}_4$ [58], $\text{Au/g-C}_3\text{N}_4/\text{Cu}_2\text{O}$ [59], and $\text{CeO}_2/\text{g-C}_3\text{N}_4$ [60], have the ability to efficiently catalyze the degradation of chromium (Cr^{6+}), Bisphenol A (BPA), and oxytetracycline hydrochloride, in addition to the formation of hydrogen.

4. Conclusions

The nanocatalytic degradation of harmful dyes methylene blue, congo red, 4-nitrophenol, and 4-nitroaniline was achieved through biosynthesized green silver nanoparticles using aqueous leaf extract of *Cestrum nocturnum* L. Based on HR-SEM and HR-TEM analysis, most of the biosynthesized green AgNPs were mostly spherical in shape. The size distribution of AgNPs was calculated with the help of DLS and TEM, which were in the range of 50–95 nm. The catalytic degradation of the selected dyes in the presence of the good reducing agent NaBH_4 was slow, which was monitored by taking absorption spectra. Biosynthesized green silver nanoparticles, when added to the reaction mixture containing

NaBH₄ and dye solution, decolorized the dyes within a short time. The correlation between the decolorization and disintegration of chromophore complex structures of the dyes was validated by the UV-Visible absorption spectra of the catalytic reduction reactions. After adding the AgNPs as a catalyst, more than 90% of the dye 4-nitrophenol and congo red were degraded within 8 and 15 min, respectively. Degradation of the dyes 4-nitroaniline and methylene blue up to 78–79% was completed in 8 and 18 min, respectively. The above results suggest that the photoinduced AgNPs have excellent catalytic activity. The catalytic degradation efficiency of biosynthesized AgNPs is supposed to be due to the presence of various primary and secondary metabolites. Thus, we can conclude that the enhanced ability of biosynthesized AgNPs for the catalytic degradation of toxic dyes will help in recycling the aquatic sources that are contaminated with toxic dyes in the future.

Author Contributions: Optimization of AgNPs green synthesis, P.K. and J.D.; Review and manuscript preparation, A.K.S. and V.D.R.; Plant material collection and extract preparation, P.V.; Supervision, experimental design, K.N.T. and S.K.M.; Manuscript preparation and editing, T.M. and S.M. All authors have read and agreed to the published version of the manuscript.

Funding: Kavindra Nath Tiwari thankfully acknowledges Banaras Hindu University, Varanasi for providing financial assistance through an incentive grant under the IoE scheme (6031) for research. The authors also acknowledge support by the laboratory «Soil Health» of the Southern Federal University with the financial support of the Ministry of Science and Higher Education of the Russian Federation, agreement No. 075-15-2022-1122.

Data Availability Statement: Not applicable.

Acknowledgments: The authors (K.N.T, P.K, J.D, P.V.) are highly grateful to the Head, Department of Botany, MMV, Banaras Hindu University, Varanasi for providing necessary facilities for doing this work and authors S.K.M and A.K.S. is highly grateful to IIT-BHU for instrumentation facilities (FTIR, DLS, HR-TEM, HR-SEM and AFM) and P.K. is grateful for the fellowship support from RGNF, UGC, New Delhi.

Conflicts of Interest: The authors declare no conflict of interest.

References

1. Jeevanandam, J.; Barhoum, A.; Chan, Y.S.; Dufresne, A.; Danquah, M.K. Review on Nanoparticles and nanostructured materials: History, sources, toxicity and regulations. *Beilstein J. Nanotechnol.* **2018**, *9*, 1050–1074. [[CrossRef](#)] [[PubMed](#)]
2. Khan, I.; Saeed, K.; Khan, I. Nanoparticles: Properties, applications and toxicities. *Arab. J. Chem.* **2019**, *12*, 908–931. [[CrossRef](#)]
3. Martinez, G.; Merinero, M.; Perez-Aranda, M.; Perez-Soriano, E.M.; Ortiz, T.; Begines, B.; Alcudia, A. Environmental impact of nanoparticles' application as an emerging technology: A Review. *Materials* **2021**, *14*, 166. [[CrossRef](#)] [[PubMed](#)]
4. Salem, S.S.; Fouda, A. Green synthesis of metallic nanoparticles and their prospective biotechnological applications: An overview. *Biol. Trace Elem. Res.* **2021**, *199*, 344–370. [[CrossRef](#)] [[PubMed](#)]
5. Rajput, V.D.; Minkina, T.; Upadhyay, S.K.; Kumari, A.; Ranjan, A.; Mandzhieva, S.; Sushkova, S.; Singh, R.K.; Verma, K.K. Nanotechnology in the restoration of polluted soil. *Nanomaterials* **2022**, *12*, 769. [[CrossRef](#)]
6. Rajput, V.D.; Singh, A.; Minkina, T.; Rawat, S.; Mandzhieva, S.; Sushkova, S.; Shuvaeva, V.; Nazarenko, O.; Rajput, P.; Komariah; et al. Nano-enabled Products: Challenges and opportunities for sustainable agriculture. *Plants* **2021**, *10*, 2727. [[CrossRef](#)]
7. Elbehiry, F.; Darweesh, M.; Al-Anany, F.S.; Khalifa, A.M.; Almashad, A.A.; El-Ramady, H.; El-Banna, A.; Rajput, V.D.; Jatav, H.S.; Elbasiouny, H. Using biochar and nano biochar of water Hyacinth and black tea waste in metals removal from aqueous solutions. *Sustainability* **2022**, *14*, 10118. [[CrossRef](#)]
8. Mukherjee, A.; Sarkar, D.; Sasmal, S. A review of green synthesis of metal nanoparticles using algae. *Front. Microbiol.* **2021**, *12*, 693899. [[CrossRef](#)]
9. Kumar, S.; Aharwal, R.P.; Sandhu, S.S. Nanoparticles from fungi: A novel approach toward eco-friendly drug designing. *Mod. Approaches Drug Des.* **2020**, *3*, 1–9.
10. Ibrahim, E.; Zhang, M.; Zhang, Y.; Hossain, A.; Qiu, W.; Chen, Y.; Wang, Y.; Wu, W.; Sun, G.; Li, B. Green-synthesization of silver nanoparticles using endophytic bacteria isolated from garlic and its antifungal activity against wheat *Fusarium* head blight pathogen *Fusarium graminearum*. *Nanomaterials* **2020**, *10*, 219. [[CrossRef](#)]
11. Husni, P.; Ramadhania, Z.M. Plant extract loaded nanoparticles. *Indonas. J. Pharm.* **2021**, *3*, 38–49. [[CrossRef](#)]
12. Vanlalveni, C.; Lallianrawna, S.; Biswas, A.; Selvaraj, M.; Changmai, B.; Rokhum, L.R. Green synthesis of silver nanoparticles using plant extracts and their antimicrobial activities: A review of recent literature. *RSC Adv.* **2021**, *11*, 2804–2837. [[CrossRef](#)]
13. Mohamad, N.A.N.; Arham, N.A.; Jai, J.; Hadi, A. Plant extract as reducing agent in synthesis of metallic nanoparticles: A review. *Adv. Mat. Res.* **2013**, *832*, 350–355. [[CrossRef](#)]

14. Umamaheswari, C.; Lakshmanan, A.; Nagarajan, N.S. Green synthesis, characterization and catalytic degradation studies of gold nanoparticles against congo red and methyl orange. *J. Photochem. Photobiol. B Biol.* **2018**, *17*, 33–39. [[CrossRef](#)]
15. Zhang, X.F.; Liu, Z.G.; Shen, W.; Gurunathan, S. Silver nanoparticles: Synthesis, characterization, properties, applications, and therapeutic approaches. *Int. J. Mol. Sci.* **2016**, *17*, 1534. [[CrossRef](#)]
16. Lellis, B.; Favaro-Polonio, C.Z.; Pamphile, J.A.; Polonio, J.C. Effects of textile dyes on health and the environment and bioremediation potential of living organisms. *Biotechnol. Res. Innov.* **2019**, *3*, 275–290. [[CrossRef](#)]
17. Lima, R.O.A.; Bazo, A.P.; Salvadori, D.M.; Rech, C.M.; Oliveira, P.D.; Umbuzeiro, G.A. Mutagenic and carcinogenic potential of a textile azo dye processing plant effluent that impacts a drinking water source. *Mutat. Res.* **2007**, *626*, 53–60. [[CrossRef](#)]
18. Nguyen, V.H.; Smith, S.M.; Wantala, K.; Kajitvichyanukul, P. Photocatalytic remediation of persistent organic pollutants (POPs): A review. *Arab. J. Chem.* **2020**, *13*, 6949–6965. [[CrossRef](#)]
19. Kobylewski, S.; Jacobson, M.F. Toxicology of food dyes. *Int. J. Occup. Environ. Health.* **2012**, *18*, 220–246. [[CrossRef](#)]
20. Sabnis, R.W. *Hand Book of Biological Dyes and Stains, Synthesis and Industrial Applications*; Wiley: Hoboken, NJ, USA, 2010; pp. 1–544.
21. Kumar, P.; Sonkar, P.; Tiwari, K.N.; Singh, A.K.; Mishra, S.K.; Dixit, J.; Ganesan, V.; Singh, J. Sensing of mercury ion using light induced aqueous leaf extract mediated green synthesized silver nanoparticles of *Cestrum nocturnum* L. *Environ. Sci. Pollut. Res.* **2022**, *29*, 79995–80004. [[CrossRef](#)]
22. Veisi, H.; Azizi, S.; Mohammadi, P. Green synthesis of the silver nanoparticles mediated by *Thymbra spicata* extract and its application as a heterogeneous and recyclable nano catalyst for catalytic reduction of a variety of dye in water. *J. Clean. Prod.* **2018**, *170*, 1536–1543. [[CrossRef](#)]
23. Mulvaney, P. Surface plasmon spectroscopy of nanosized metal particles. *Langmuir* **1996**, *12*, 788–800. [[CrossRef](#)]
24. Singh, C.; Kumar, J.; Kumar, P.; Chauhan, B.S.; Tiwari, K.N.; Mishra, S.K.; Srikrishna, S.; Saini, R.; Nath, G.; Singh, J. Green synthesis of silver nanoparticles using aqueous leaf extract of *Premna integrifolia* (L.) rich in polyphenols and evaluation of their antioxidant, antibacterial and cytotoxic activity. *Biotechnol. Biotechnol. Equip.* **2019**, *33*, 359–371. [[CrossRef](#)]
25. Noh, C.H.C.; Azmin, N.F.M.; Amid, A. Principal component analysis application on flavonoids characterization. *Adv. Sci. Technol. Eng. Syst. J.* **2017**, *2*, 435–440. [[CrossRef](#)]
26. Heneczowski, M.; Kopacz, M.; Nowak, D.; Kuzniar, A. Infrared spectrum analysis of some flavonoids. *Acta Pol. Pharm.* **2001**, *58*, 415–420. [[PubMed](#)]
27. Kumar, V.; Yadav, S.K. Plant mediated synthesis of silver and gold nanoparticles and their applications. *J. Chem. Technol. Biotechnol.* **2009**, *84*, 151–157. [[CrossRef](#)]
28. Jeeva, K.; Thiagarajan, M.; Elangovan, V.; Geetha, N.; Venkatachalam, P. *Caesalpinia coriaria* leaf extracts mediated biosynthesis of metallic silver nanoparticles and their antibacterial activity against clinically isolated pathogens. *Ind. Crop. Prod.* **2014**, *52*, 714–720. [[CrossRef](#)]
29. Yusuf, S.N.A.M.; Mood, C.N.A.C.; Ahmad, N.H.; Sandai, D.; Lee, C.K.; Lim, V. Optimization of biogenic synthesis of silver nanoparticles from flavonoid-rich *Clinacanthus nutans* leaf and stem aqueous extracts. *R. Soc. Open Sci.* **2020**, *7*, 200065.
30. Das, G.; Patra, J.K.; Debnath, T.; Ansari, A.; Shin, H.S. Investigation of antioxidant, antibacterial, antidiabetic, and cytotoxicity potential of silver nanoparticles synthesized using the outer peel extract of *Ananas comosus* (L.). *PLoS ONE* **2019**, *14*, e0220950. [[CrossRef](#)]
31. Awwad, A.M.; Salem, N.M.; Abdeen, A.O. Green synthesis of silver nanoparticles using carob leaf extract and its antibacterial activity. *Int. J. Ind. Chem.* **2013**, *4*, 29. [[CrossRef](#)]
32. Venugopal, K.; Rather, H.A.; Rajagopal, K.; Shanthi, M.P.; Sheriff, K.; Illiyas, M.; Rather, R.A.; Manikandan, E.; Uvarajan, S.; Bhaskar, M.; et al. Synthesis of silver nanoparticles (AgNPs) for anticancer activities (MCF 7 breast and A549 lung cell lines) of the crude extract of *Syzygium aromaticum*. *J. Photochem. Photobiol. B Biol.* **2016**, *167*, 282–289. [[CrossRef](#)] [[PubMed](#)]
33. Kumar, V.; Singh, D.K.; Mohan, S.; Hasan, S.H. Photo-induced biosynthesis of silver nanoparticles using aqueous extract of *Erigeron bonariensis* and its catalytic activity against acridine orange. *J. Photochem. Photobiol. B Biol.* **2016**, *155*, 39–50. [[CrossRef](#)] [[PubMed](#)]
34. Bolean, M.; Borin, I.A.; Simao, A.M.S.; Bottini, M.; Bagatolli, L.A.; Hoylaerts, M.F.; Millan, J.L.; Ciancaglini, P. Topographic analysis by atomic force microscopy of proteo liposomes matrix vesicle mimetics harboring TNAP and AnxA5. *Biochim. Biophys. Acta. Biomembr.* **2017**, *1859*, 1911–1920. [[CrossRef](#)] [[PubMed](#)]
35. Ahmad, V.U.; Fehmida, T.; Baqai, F.T.; Fatima, I.; Ahmad, R. A spirostanol glycoside from *Cestrum nocturnum*. *Phytochemistry* **1991**, *30*, 3057–3061. [[CrossRef](#)]
36. Mimaki, Y.; Watanabe, K.; Sakagami, H.; Sashida, Y. Steroidal glycosides from the leaves of *Cestrum nocturnum*. *J. Nat. Prod.* **2002**, *65*, 1863–1868. [[CrossRef](#)]
37. Gade, A.; Gaikwad, S.; Duran, N.; Rai, M. Green synthesis of silver nanoparticles by *Phoma glomerata*. *Micron* **2014**, *59*, 52–59. [[CrossRef](#)]
38. Mathur, M. Properties of phyto-reducing agents utilize for production of nano-particles, existing knowledge and gap. *Int. J. Pure Appl. Biosci.* **2014**, *2*, 113–130.
39. Benkhaya, S.; Rabet, S.M.; Harfi, A.E. A review on classifications, recent synthesis and applications of textile dyes. *Inorg. Chem. Commun.* **2020**, *115*, 107891. [[CrossRef](#)]
40. Adane, T.; Adugna, A.M.; Alemayehu, E. Textile industry effluent treatment techniques. *J. Chem.* **2021**, *2021*, 5314404. [[CrossRef](#)]

41. Mehta, M.; Sharma, M.; Pathania, K.; Jena, P.K.; Bhusan, I. Degradation of synthetic dyes using nanoparticles: A mini-review. *Environ. Sci. Pollut. Res.* **2021**, *28*, 7898–7909. [[CrossRef](#)]
42. Kora, A.J.; Rastogi, L. Green synthesis of palladium nanoparticle using gum ghatti (*Anogeissus latifolia*) and its application as an antioxidant and catalyst. *Arab. J. Chem.* **2015**, *11*, 1097–1106. [[CrossRef](#)]
43. Edison, T.J.I.; Sethuraman, M.G. Instant green synthesis of silver nanoparticles using *Terminalia chebula* fruit extract and evaluation of their catalytic activity on reduction of methylene blue. *Process Biochem.* **2012**, *47*, 1351–1357. [[CrossRef](#)]
44. Suvith, V.S.; Philip, D. Catalytic degradation of methylene blue using biosynthesized gold and silver nanoparticles. *Spectrochim. Acta A Mol. Biomol. Spectrosc.* **2014**, *118*, 526–532. [[CrossRef](#)]
45. Saravanan, C.; Rajesh, R.; Kaviarasan, T.; Muthukumar, K.; Kavitate, D.; Shetty, P.H. Synthesis of silver nanoparticles using bacterial exopolysaccharide and its application for degradation of azo-dyes. *Biotechnol. Rep.* **2017**, *15*, 33–40. [[CrossRef](#)]
46. Mohanty, A.S.; Jena, B.S. Innate catalytic and free radical scavenging activities of silver nanoparticles synthesized using *Dillenia indica* bark extract. *J. Colloid Interface Sci.* **2017**, *496*, 513–521. [[CrossRef](#)]
47. Atarod, M.; Nasrollahzadeh, M.; Sajadi, M.S. *Euphorbia heterophylla* leaf extract mediated green synthesis of Ag/TiO₂ nanocomposite and investigation of its excellent catalytic activity for reduction of variety of dyes in water. *J. Colloid Interface Sci.* **2016**, *462*, 272–279. [[CrossRef](#)]
48. Mubiayi, M.P.; Muleja, A.A.; Nzaba, S.K.M.; Mamba, B.B. Geochemical and physicochemical characteristics of clay materials from congo with photocatalytic activity on 4-Nitrophenol in aqueous solutions. *ACS Omega* **2020**, *5*, 29943–29954. [[CrossRef](#)]
49. Booth, G. *Nitro Compounds, Aromatic*. *Ullmann's Encyclopedia of Industrial Chemistry*; Wiley-VCH: Weinheim, Germany, 2007.
50. Sarvalkar, P.D.; Rutuja, R.M.; Nimbalkar, M.S.; Sharma, K.K.; Patil, P.S.; Kamble, G.S.; Neeraj, R.; Prasad, N.R. Bio-mimetic synthesis of catalytically active nano-silver using *Bostaurus* (A-2) urine. *Sci. Rep.* **2021**, *11*, 16934. [[CrossRef](#)]
51. Kolya, H.; Maiti, P.; Pandey, A.; Tripathy, T. Green synthesis of silver nanoparticles with antimicrobial and azo dye (Congo red) degradation properties using *Amaranthus gangeticus* Linn leaf extract. *J. Anal. Sci. Technol.* **2015**, *6*, 33. [[CrossRef](#)]
52. Edison, T.N.J.I.; Atchudan, R.; Sethuraman, M.G.; Lee, Y.R. Reductive-degradation of carcinogenic azo dyes using *Anacardium occidentale* testa derived silver nanoparticles. *J. Photochem. Photobiol. B* **2016**, *162*, 604–610. [[CrossRef](#)]
53. Choudhary, M.K.; Kataria, J.; Sharma, S. Retraction: Evaluation of the kinetic and catalytic properties of biogenically synthesized silver nanoparticles. *J. Clean. Prod.* **2018**, *198*, 882–890. [[CrossRef](#)]
54. Jain, N.; Jain, P.; Rajput, D.; Patil, U.K. Green synthesized plant-based silver nanoparticles: Therapeutic prospective for anticancer and antiviral activity. *Micro Nano Syst. Lett.* **2021**, *9*, 5. [[CrossRef](#)]
55. Nasrollahzadeh, M.; Atarod, M.; Jaleh, B.; Gandomirouzbahani, M. In situ green synthesis of Ag nanoparticles on grapheme oxide/TiO₂ nanocomposite and their catalytic activity for the reduction of 4-nitrophenol, congo red and methylene blue. *Ceram. Int.* **2016**, *42*, 8587–8596. [[CrossRef](#)]
56. Fairuzi, A.A.; Bonnia, N.N.; Akhir, R.M.; Abrani, M.A.; Akil, H.M. Degradation of methylene blue using silver nanoparticles synthesized from *Imperata cylindrica* aqueous extract. *IOP Conf. Ser. Earth Environ. Sci.* **2018**, *105*, 012018. [[CrossRef](#)]
57. Moon, S.A.; Salunke, B.K.; Saha, P.; Deshmukh, A.R.; Kim, B.S. Comparison of dye degradation potential of biosynthesized copper oxide, manganese dioxide, and silver nanoparticle using *Kalopanax pictus* plant extract. *Korean J. Chem. Eng.* **2018**, *35*, 702–708. [[CrossRef](#)]
58. Zhao, W.; Ma, S.; Yang, G.; Wang, G.; Zhang, L.; Xia, D.; Huang, H.; Cheng, Z.; Xu, J.; Sun, C.; et al. Z-scheme Au decorated carbon nitride/cobalt tetroxide plasmonic heterojunction photocatalyst for catalytic reduction of hexavalent chromium and oxidation of Bisphenol A. *J. Hazard. Mater.* **2021**, *410*, 124539. [[CrossRef](#)]
59. Mu, F.; Miao, X.; Cao, J.; Zhao, W.; Yang, G.; Zeng, H.; Li, S.; Sun, C. Integration of plasmonic effect and S-scheme heterojunction into gold decorated carbon nitride/cuprous oxide catalyst for photocatalysis. *J. Clean. Prod.* **2022**, *360*, 131948. [[CrossRef](#)]
60. Zhao, W.; She, T.; Zhang, J.; Wang, G.; Zhang, S.; Wei, W.; Yang, G.; Zhang, L.; Dehua Xia, D.; Cheng, Z.; et al. A novel z-scheme ceo2/g-c3n4 heterojunction photocatalyst for degradation of bisphenol a and hydrogen evolution and insight of the photocatalysis mechanism. *J. Mater. Sci. Technol.* **2021**, *85*, 18–29. [[CrossRef](#)]